Supplement of Atmos. Chem. Phys., 21, 8531–8555, 2021
https://doi.org/10.5194/acp-21-8531-2021-supplement

Atmospheric Chemistry and Physics
Open Access
EGU

Supplement of

Measurement report: Molecular composition, optical properties, and radiative effects of water-soluble organic carbon in snowpack samples from northern Xinjiang, China

Yue Zhou et al.

Correspondence to: Alexander Laskin (alaskin@purdue.edu) and Xin Wang (wxin@lzu.edu.cn)

Table of Contents

S1. Assessment of the efficiency of SPE.

Because original samples and the eluents were in different solvents (water and ACN, respectively), it is hard to compare their UV-Vis absorbance directly to estimate recoveries. We used a two-step method to assess the efficiency of SPE. First, the absorbances of original samples and effluents were measured to make sure that most of light-absorbing organics were retained on cartridges. In this step, the absorbances of effluents at 280 nm (Abs_{280}) only accounted for 16% of original samples on average. Then, we eluted the analytes twice by ACN to obtain eluents 1 and 2, and recorded their absorbances. Overall, The Abs_{280} values of eluents 2 were 27% of that for eluents1 on average. Therefore, we demonstrate that this SPE method is efficient. Finally, we combined eluents 1 and 2 as analytes and concentrated them by pure N_2.

S2. Identification of adduct ions.

The following adduct ions were identified and removed, for ESI-: $[M+ACN]^-$, 41.0266 *m/z*; $[M+CH_2O_2]^-$, 46.0055 *m/z*; for ESI+: $[M+Na-H]^+$, 21.9825 *m/z*; $[M+K-H]^+$, 37.9559 *m/z*; $[M+NH_3]^+$, 17.0265 *m/z*; $[M+ACN]^+$, 41.0266 *m/z*; $[M+CH_2O_2]^+$, 46.0055 *m/z*; $[M+CHO_2Na]^+$, 67.9874 *m/z*. Note that [M] represents $[Molecule - H]^-$ in ESI- and $[Molecule + H]^+$ in ESI+. In addition to mass differences, the following constrains were applied as well: retention time tolerance of 0.1 min; mass tolerance of 3 ppm; max adduct peak height of 50% (Wang et al., 2017).

Table S1. Classification scheme of sampling sites.

Group name	Sites	Number of sites
Urban/Industrial	106-118, and 131	14
Rural/remote	119, 121-125, and 127-130	10
Soil-influenced	104, 105, and 126	3
Site 120	120	1

Table S2. Averages (arithmetic mean ± standard deviation) of chemical species and optical properties for each group of samples. The soluble ions are shown in the mass fractions of total ion mass. The fluorescence components are shown in the relative contributions to the total fluorescence intensity.

	Urban/Industrial (n = 14)	Rural/Remote (n = 10)	Soil-influenced (n = 3)	Site 120 (n = 1)
Soluble ions				
$\%Na^+$	5±3	4±3	3±1	4
$\%NH_4^+$	9±4	6±5	2±1	3
$\%K^+$	2±1	3±1	6±2	4
$\%Mg^{2+}$	1±1	1±0.3	2±0.1	1
$\%Ca^{2+}$	22±9	16±8	50±4	20
$\%Cl^-$	7±3	7±3	3±1	5
$\%SO_4^{2-}$	33±7	18±7	17±2	20
$\%NO_3^-$	22±10	45±9	16±2	43
Other chemical species				
BC (ng g^{-1}) [a]	707±651	119±63	440±121	44
WSOC (ng g^{-1})	1968±953	885±328	2082±1438	7069
Optical properties				
MAC_{300} (m^2 g^{-1})	1.32±0.24	1.02±0.21	2.75±0.99	1.95
MAC_{365} (m^2 g^{-1})	0.39±0.11	0.38±0.12	0.94±0.31	0.95
MAC_{405} (m^2 g^{-1})	0.21±0.07	0.19±0.07	0.45±0.14	0.16
$AAE_{330\text{-}400}$	6.0±0.8	5.4±0.7	6.4±0.3	12.3
%HULIS-1	23±7	14±4	49±9	19
%HULIS-2	46±9	38±6	32±1	38
%PRLIS	30±9	48±5	19±10	44

[a] Shi et al. (2020)

Table S3. Summary of concentrations of chemical species and optical properties of WSOC at each site.

Site No.	Na^+	$NH4^+$	K^+	Mg^{2+}	Ca^{2+}	Cl^-	SO_4^{2-}	NO_3^-
	mg L^{-1}	mg L^{-1}	mg L^{-1}	mg L^{-1}	mg L^{-1}	mg L^{-1}	mg L^{-1}	mg L^{-1}
104	0.31	0.23	1.13	0.30	6.36	0.34	2.59	1.73
105	0.15	0.09	0.13	0.07	1.35	0.14	0.46	0.53
106	0.38	0.93	0.28	0.19	2.42	0.52	3.26	6.02
107[a]	1188	3.90	25.6	186	57.3	449	996	12.8
108	0.39	0.99	0.25	0.21	4.84	1.38	4.73	3.57
109	0.75	1.28	0.35	0.41	8.85	1.03	15.10	6.20
110	2.97	0.88	0.24	0.19	2.74	2.33	8.15	5.72
111	0.43	0.91	0.21	0.18	2.64	0.71	3.68	6.97
112	0.32	0.39	0.15	0.08	1.64	0.28	1.37	0.88
113	0.60	3.45	0.34	0.17	3.95	1.09	8.82	5.31
114	1.19	3.63	0.44	0.32	4.56	2.14	11.67	7.95
115	0.19	2.69	0.26	0.08	1.91	0.58	4.98	3.23
116	1.60	2.52	0.43	0.47	10.48	2.26	8.87	2.87
117	0.24	0.72	0.17	0.18	2.99	0.31	1.94	1.35
118	3.75	1.76	0.55	1.55	11.04	6.74	15.47	3.74
119	0.16	0.93	0.18	0.04	0.45	0.38	0.04	2.56
120	0.08	0.06	0.08	0.02	0.41	0.10	0.41	0.89
121	0.24	0.14	0.12	0.04	0.35	0.35	0.80	1.16
122	0.16	0.37	0.19	0.09	1.04	0.25	1.70	2.49
123	0.04	0.08	0.10	0.03	0.33	0.10	0.49	1.30
124	0.05	0.10	0.10	0.02	0.33	0.10	0.46	1.05
125	0.09	0.16	0.12	0.04	1.16	0.11	0.50	0.83
126	0.10	0.04	0.18	0.08	1.99	0.08	0.55	0.62
127	0.72	0.24	0.21	0.06	1.08	1.05	1.09	2.65
128	0.31	0.29	0.16	0.05	0.54	0.50	1.17	3.41
129	0.16	0.52	0.21	0.11	1.19	0.33	1.55	3.98
130	0.15	0.30	0.18	0.09	1.17	0.45	1.35	4.38
131	2.04	4.32	0.61	0.50	5.47	3.31	16.12	5.92

[a] Sample of site 107 was collected on a frozen salty lake, leading to very high soluble ion concentrations.

Table S3. Continue.

Site No.	WSOC	BC	MAC_{300}	MAC_{365}	MAC_{405}	AAE	HULIS-1	HULIS-2	PRLIS
	ng g^{-1}	ng g^{-1}	m^2 g^{-1}	m^2 g^{-1}	m^2 g^{-1}	330-400	%	%	%
104	4106	595	4.13	1.39	0.65	6.8	62	33	5
105	899	298	2.18	0.73	0.36	6.5	42	31	27
106	1357	276	0.87	0.20	0.10	6.9	18	39	43
107[a]	4429	282	1.26	0.28	0.14	7.1	35	45	20
108	1346	318	1.29	0.41	0.22	5.8	32	37	31
109	1958	585	1.36	0.41	0.21	6.1	32	39	28
110	1451	440	0.77	0.19	0.09	6.7	11	44	45
111	1561	315	1.38	0.30	0.14	7.4	15	47	38
112	664	100	1.44	0.58	0.32	4.7	26	27	47
113	2558	328	1.51	0.42	0.23	6.1	21	59	20
114	2228	1318	1.62	0.47	0.27	5.7	19	59	22
115	776	215	1.22	0.42	0.21	5.3	21	44	35
116	2290	1852	1.30	0.41	0.28	4.3	20	50	30
117	1384	224	1.67	0.54	0.30	5.4	24	52	24
118	2461	1827	1.44	0.48	0.24	6.0	32	47	21
119	878	89	1.21	0.40	0.19	6.6	8	49	43
120	7069	44	1.95	0.95	0.16	12.3	19	38	44
121	616	77	1.04	0.38	0.19	5.2	11	39	50
122	980	254	1.07	0.35	0.17	6.0	18	44	38
123	671	86	1.19	0.47	0.23	5.5	14	39	47
124	478	42	1.06	0.47	0.23	4.5	13	28	59
125	566	79	1.42	0.62	0.34	4.5	21	32	47
126	1241	427	1.93	0.71	0.35	6.0	44	31	25
127	1099	199	0.86	0.32	0.16	5.2	20	35	45
128	1637	121	0.61	0.19	0.09	5.7	12	39	49
129	1135	81	0.85	0.26	0.12	5.8	15	36	49
130	791	163	0.91	0.33	0.18	4.5	11	35	55
131	3085	1823	1.39	0.40	0.22	5.9	20	60	20

Table S4. Descriptions of fluorescent components identified by PARAFAC analysis. The secondary peaks are shown in parentheses.

Component number	Excitation maximal wavelength (nm)	Emission maximal wavelength (nm)	Descriptions	References
C1 (HULIS-1)	244 (304)	460	Terrestrial HULIS, highly-oxygenated organic aerosols	Chen et al., 2016a,b;Stedmon et al., 2003
C2 (HULIS-2)	<240 (297)	395	Marine, microbial, or anthropogenic (industrial) HULIS	Chen et al., 2020;Coble, 1996;Stedmon and Markager, 2005;Zhang et al., 2010
C3 (PRLIS)	269	309	Tyrosine-like fluorophore	Coble et al., 1998;Yu et al., 2015

Table S5. Input parameters for the SNICAR model.

Site	Snow depth	Snow radius	Snow density	Solar zenith angle	BC[a]	WSOC
	cm	μm	kg m^{-3}	degree	ng g^{-1}	ng g^{-1}
104	8.0	429	200	72.03	595	4106
105	22.0	214	250	72.08	298	899
106	7.0	269	130	71.72	276	1357
107	5.5	155	120	71.59	282	4429
108	7.0	329	130	71.00	318	1346
109	8.0	224	120	71.24	585	1958
110	4.0	506	180	71.24	440	1451
111	7.0	179	110	71.16	315	1561
112	19.0	111	180	70.73	100	664
113	21.0	135	220	70.77	328	2558
114	6.0	119	110	71.00	1318	2228
115	8.0	122	180	70.49	215	776
116	9.5	180	120	70.25	1852	2290
117	20.0	109	120	70.04	224	1384
118	16.0	287	250	70.12	1827	2461
119	4.5	140	100	70.53	89	878
120	12.5	142	120	72.31	44	7069
121	8.0	193	160	72.91	77	616
122	3.5	189	180	73.16	254	980
123	8.0	170	210	73.57	86	671
124	5.0	184	210	73.09	42	478
125	6.0	201	200	72.75	79	566
126	13.0	312	210	72.80	427	1241
127	6.5	214	175	72.40	199	1099
128	4.5	199	160	72.08	121	1637
129	3.0	161	130	71.71	81	1135
130	8.0	215	220	71.37	163	791
131	17.0	167	190	70.35	1823	3085

[a]Shi et al. (2020)

Table S6. The Pearson's correlation coefficients (r) for relative intensities of PARAFAC components and relative mass fractions of three soluble ions. Note: * denotes $p<0.01$.

	SO_4^{2-}	NO_3^-	Ca^{2+}
HULIS-1	0.09	-0.68*	0.73*
HULIS-2	0.51*	-0.22	-0.36
PRLIS	-0.44	0.78*	-0.42

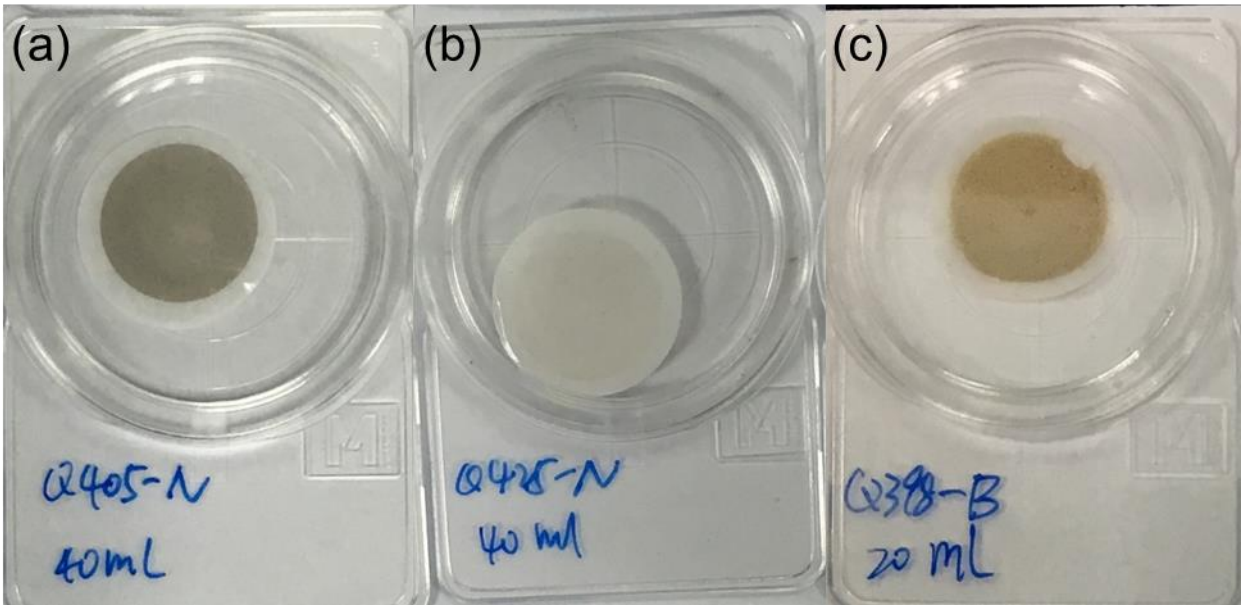

Figure S1. Filters for typical (a) urban, (b) rural, and (c) soil-influenced samples.

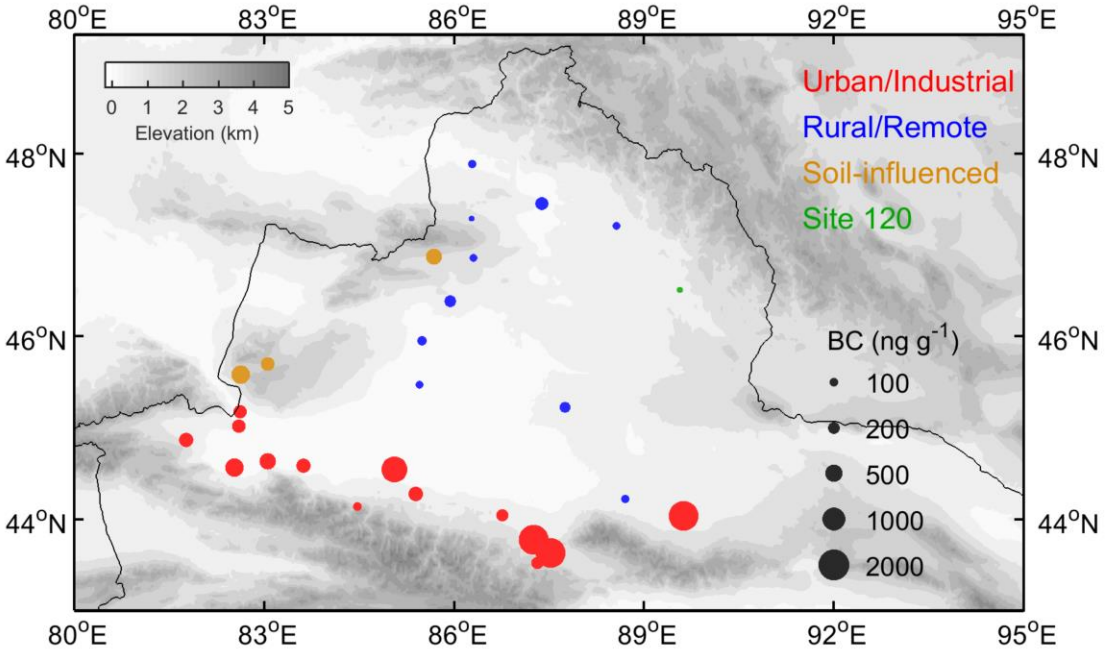

Figure S2. Spatial distribution of BC concentrations in snow. Sampling sites are divided into four groups indicated by different colors. The bubble sizes are proportional to the BC concentrations. BC data is from Shi et al. (2020).

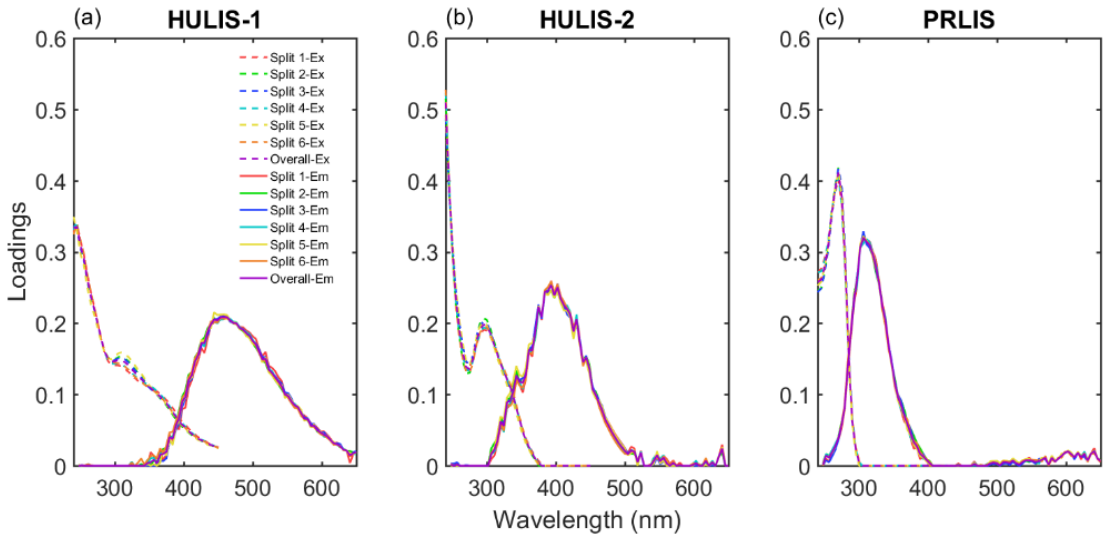

Figure S3. Split-half analysis of three-component PARAFAC model with the split style of "S4C6T3".

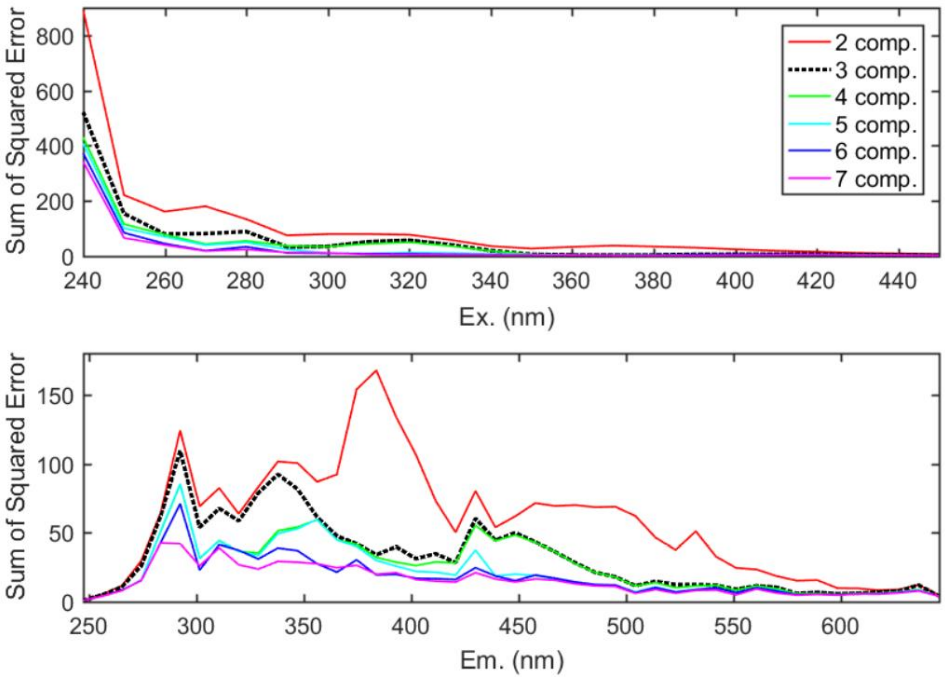

Figure S4. Residual analysis of two- to seven-component PARAFAC models, (a) excitation wavelength and (b) emission wavelength.

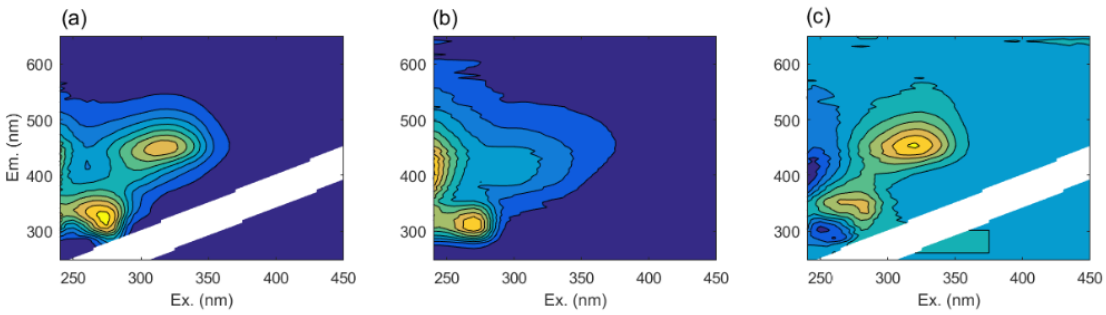

Figure S5. Results of 3-component PARAFAC analysis for sample from site 120. (a) The raw EEM. (b) The PARAFAC-modeled EEM. (c) Model residuals.

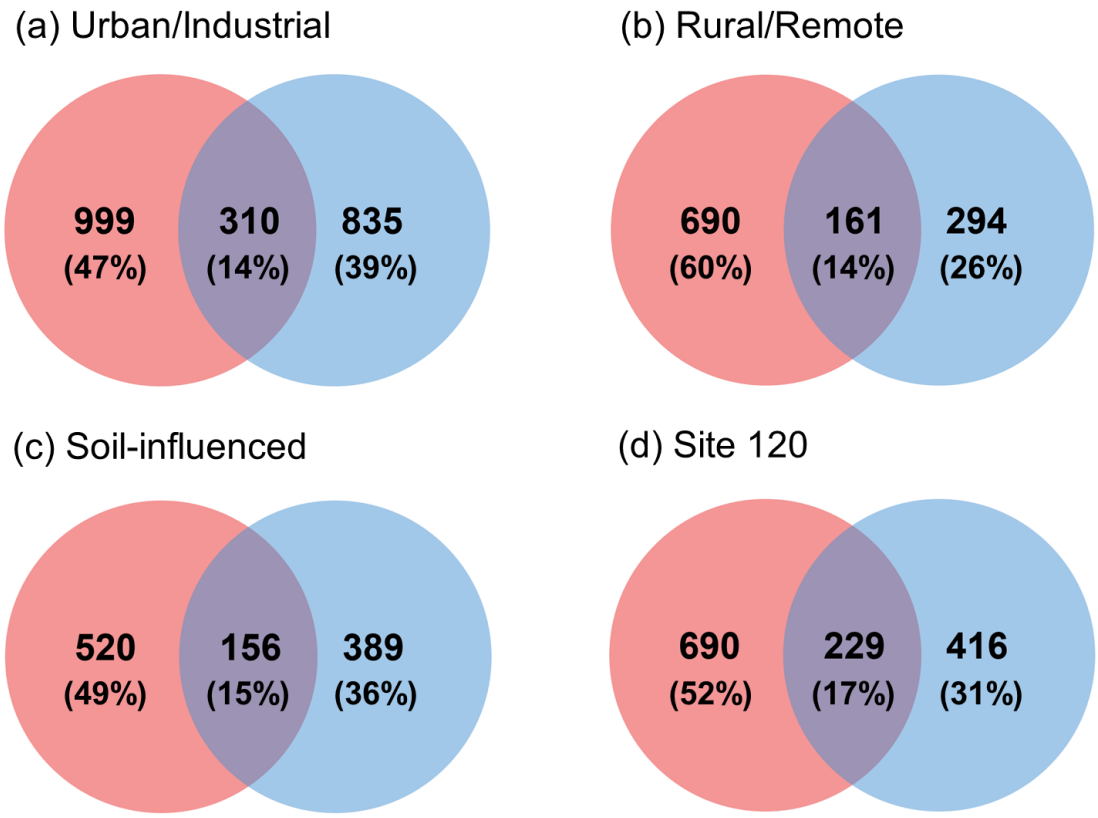

Figure S6. Venn diagrams showing the comparison of identified formulas between ESI+ (red) and ESI- (blue) for representative samples from different groups.

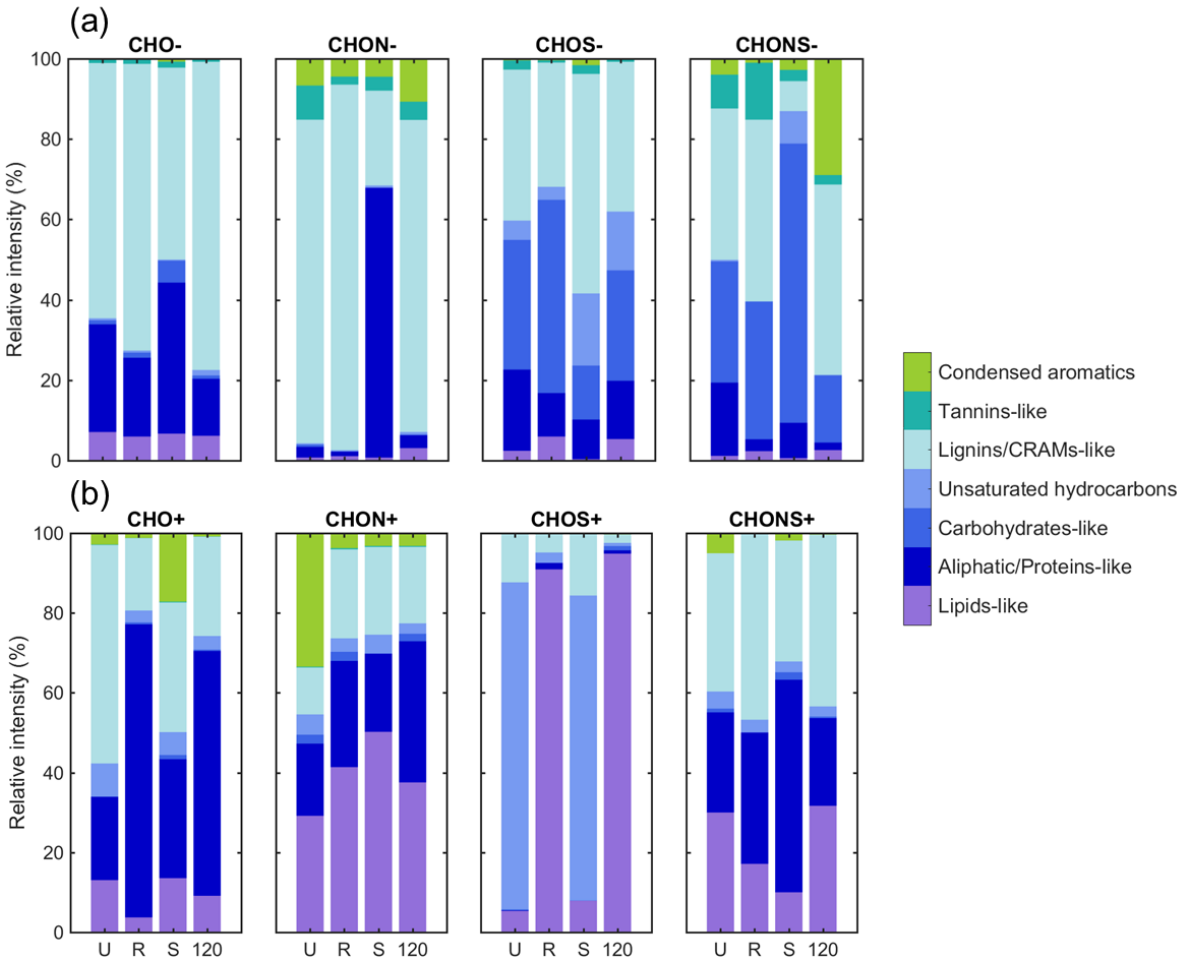

Figure S7. The relative intensities of seven chemical species to four major formula categories in (a) ESI- and (b) ESI+.

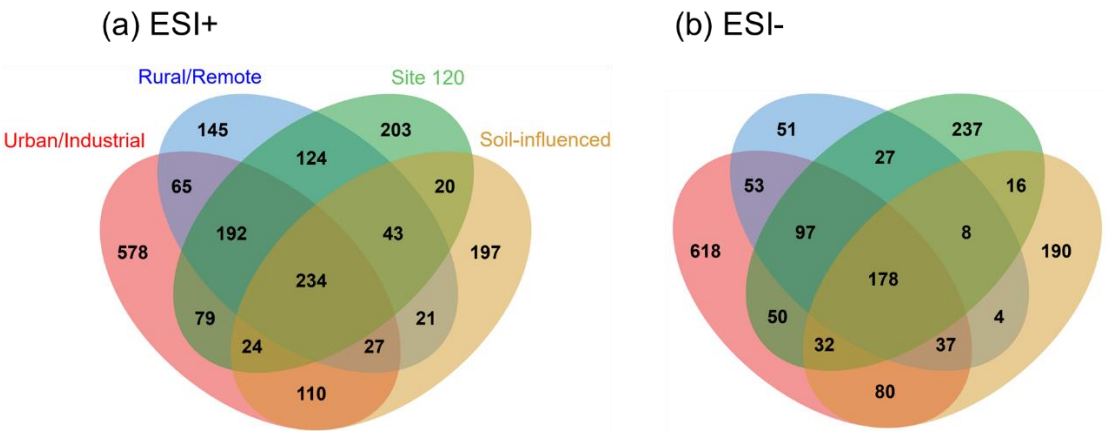

Figure S8. Venn diagrams showing the overlap and specificity for formulas detected in (a) ESI+ and (b)ESI- of representative samples from different groups.

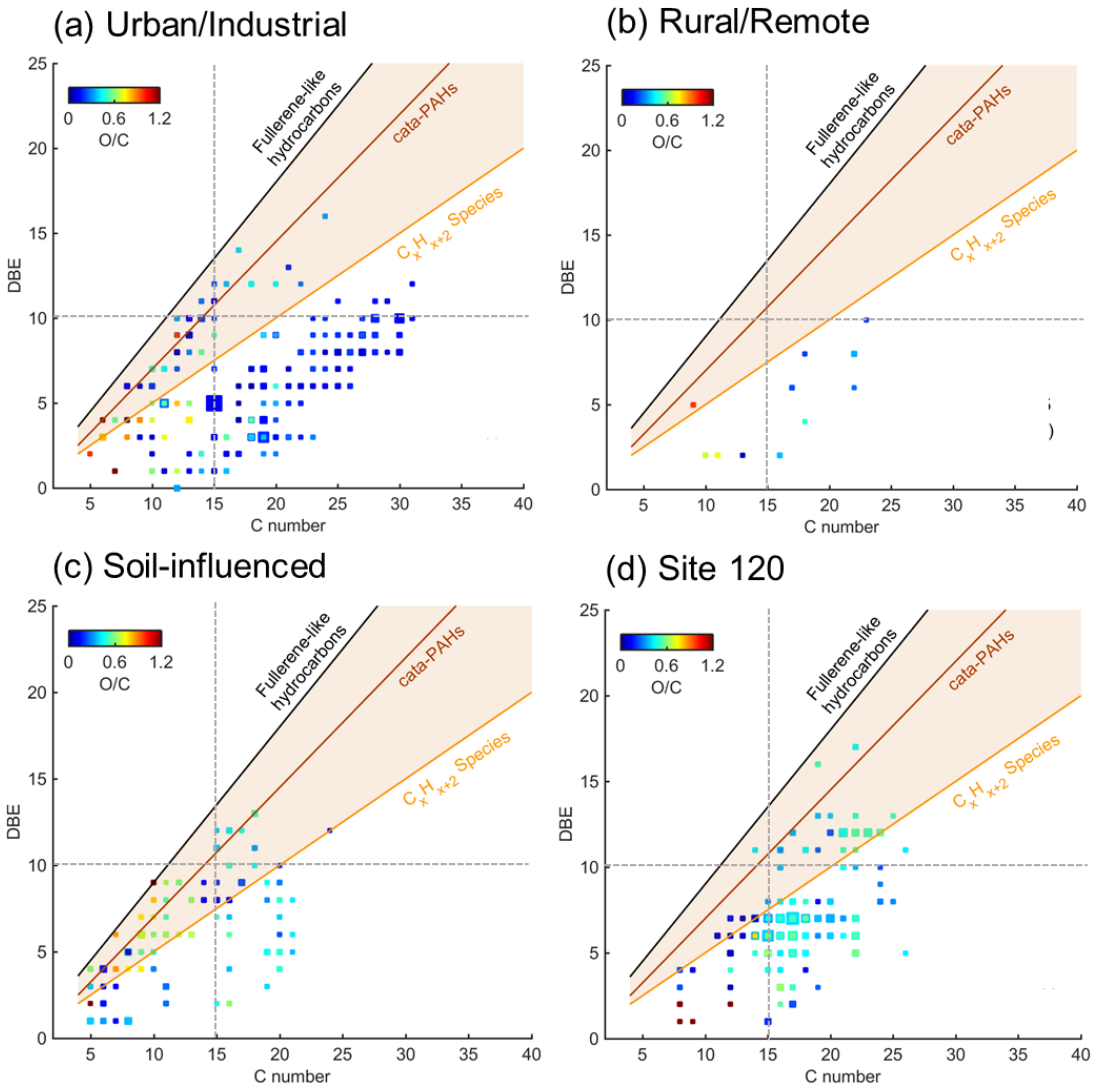

Figure S9. DBE vs. C number for unique CHO- molecules in representative samples from different groups. The reference lines indicate linear polyenes (C_xH_{x+2}, DBE = 0.5 × C), cata-condensed PAHs (DBE = 0.75 × C − 0.5), and fullerene-like hydrocarbons (DBE = 0.9 × C). Markers in the shaded area are potential BrC chromophores. The size of each marker is proportional to its relative intensity and marks are color coded by O/C ratios.

References

Chen, Q., Li, J., Hua, X., Jiang, X., Mu, Z., Wang, M., Wang, J., Shan, M., Yang, X., Fan, X., Song, J., Wang, Y., Guan, D., and Du, L.: Identification of species and sources of atmospheric chromophores by fluorescence excitation-emission matrix with parallel factor analysis, Sci. Total Environ., 718, 137322, 10.1016/j.scitotenv.2020.137322, 2020.

Chen, Q. C., Ikemori, F., and Mochida, M.: Light Absorption and Excitation-Emission Fluorescence of Urban Organic Aerosol Components and Their Relationship to Chemical Structure, Environ. Sci. Technol., 50, 10859-10868, 10.1021/acs.est.6b02541, 2016a.

Chen, Q. C., Miyazaki, Y., Kawamura, K., Matsumoto, K., Coburn, S., Volkamer, R., Iwamoto, Y., Kagami, S., Deng, Y. G., Ogawa, S., Ramasamy, S., Kato, S., Ida, A., Kajii, Y., and Mochida, M.: Characterization of Chromophoric Water-Soluble Organic Matter in Urban, Forest, and Marine Aerosols by HR-ToF-AMS Analysis and Excitation Emission Matrix Spectroscopy, Environ. Sci. Technol., 50, 10351-10360, 10.1021/acs.est.6b01643, 2016b.

Coble, P. G.: Characterization of marine and terrestrial DOM in seawater using excitation emission matrix spectroscopy, Mar. Chem. , 51, 325-346, 10.1016/0304-4203(95)00062-3, 1996.

Coble, P. G., Del Castillo, C. E., and Avril, B.: Distribution and optical properties of CDOM in the Arabian Sea during the 1995 Southwest Monsoon, Deep-Sea Res. Pt. II, 45, 2195-2223, 10.1016/S0967-0645(98)00068-X, 1998.

Shi, T., Pu, W., Zhou, Y., Cui, J., Zhang, D., and Wang, X.: Albedo of Black Carbon-Contaminated Snow Across Northwestern China and the Validation With Model Simulation, J. Geophys. Res. Atmos., 125, 10.1029/2019jd032065, 2020.

Stedmon, C. A., Markager, S., and Bro, R.: Tracing dissolved organic matter in aquatic environments using a new approach to fluorescence spectroscopy, Mar. Chem., 82, 239-254, 10.1016/S0304-4203(03)00072-0, 2003.

Stedmon, C. A., and Markager, S.: Tracing the production and degradation of autochthonous fractions of dissolved organic matter by fluorescence analysis, Limnol. Oceanogr., 50, 1415-1426, 10.4319/lo.2005.50.5.1415, 2005.

Wang, X., Hayeck, N., Brüggemann, M., Yao, L., Chen, H., Zhang, C., Emmelin, C., Chen, J., George, C., and Wang, L.: Chemical Characteristics of Organic Aerosols in Shanghai: A Study by Ultrahigh-Performance Liquid Chromatography Coupled With Orbitrap Mass Spectrometry, J. Geophys. Res. Atmos., 122, 11,703-711,722, 10.1002/2017jd026930, 2017.

Yu, H. R., Liang, H., Qu, F. S., Han, Z. S., Shao, S. L., Chang, H. Q., and Li, G. B.: Impact of dataset diversity on accuracy and sensitivity of parallel factor analysis model of dissolved organic matter fluorescence excitation-emission matrix, Sci. Rep., 5, 10207, 10.1038/Srep10207, 2015.

Zhang, Y. L., Zhang, E. L., Yin, Y., van Dijk, M. A., Feng, L. Q., Shi, Z. Q., Liu, M. L., and Qin, B. Q.: Characteristics and sources of chromophoric dissolved organic matter in lakes of the Yungui Plateau, China, differing in trophic state and altitude, Limnol. Oceanogr., 55, 2645-2659, 10.4319/lo.2010.55.6.2645, 2010.